NANO LETTERS
Cite This: Nano Lett. 2019, 19, 8201−8206
Letter
pubs.acs.org/NanoLett

Tuning Single-Atom Electron Spin Resonance in a Vector Magnetic Field

Philip Willke,[†,‡,⊥] Aparajita Singha,[†,‡,⊥] Xue Zhang,[†,‡,⊥] Taner Esat,[†,‡] Christopher P. Lutz,[§] Andreas J. Heinrich,[*,†,∥] and Taeyoung Choi[*,†,∥]

[†]Center for Quantum Nanoscience, Institute for Basic Science (IBS), Seoul 03760, Republic of Korea
[‡]Ewha Womans University, Seoul 03760, Republic of Korea
[§]IBM Almaden Research Center, San Jose, California 95120 United States
[∥]Department of Physics, Ewha Womans University, Seoul 03760, Republic of Korea

Supporting Information

ABSTRACT: Spin resonance of single spin centers bears great potential for chemical structure analysis, quantum sensing, and quantum coherent manipulation. Essential for these experiments is the presence of a two-level spin system whose energy splitting can be chosen by applying a magnetic field. In recent years, a combination of electron spin resonance (ESR) and scanning tunneling microscopy (STM) has been demonstrated as a technique to detect magnetic properties of single atoms on surfaces and to achieve sub-microelectronvolts energy resolution. Nevertheless, up to now the role of the required magnetic fields has not been elucidated. Here, we perform single-atom ESR on individual Fe atoms adsorbed on magnesium oxide (MgO) using a two-dimensional vector magnetic field as well as the local field of the magnetic STM tip in a commercially available STM. We show how the ESR amplitude can be greatly improved by optimizing the magnetic fields, revealing in particular an enhanced signal at large in-plane magnetic fields. Moreover, we demonstrate that the stray field from the magnetic STM tip is a versatile tool. We use it here to drive the electron spin more efficiently and to perform ESR measurements at constant frequency by employing tip-field sweeps. Lastly, we show that it is possible to perform ESR using only the tip field, under zero external magnetic field, which promises to make this technique available in many existing STM systems.

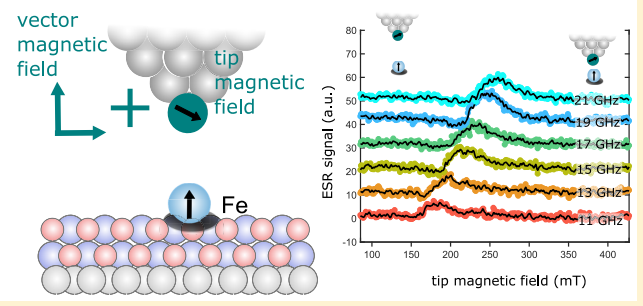

KEYWORDS: *Scanning tunneling microscopy, electron spin resonance, vector magnetic field, single-atom magnetism, magnetic sensing*

The combination of scanning probe methods and coherent control of spin systems has provided unique access to quantum systems, for instance, using nitrogen-vacancy (NV)-centers or magnetic resonance force microscopy,[1,2] enabling complex magnetic structures to be visualized.[3−6] In recent years, the combination of electron spin resonance (ESR) and scanning tunneling microscopy (STM) has entered as another platform for controlling atomic spins on surfaces.[7] This technique permits the study of magnetic interaction between pairs of atoms with unprecedented resolution[8,9] and the investigation of the phase coherent properties of atomic spins.[10,11] It even allows access to the hyperfine interaction of single atoms.[12,13] It has spiked strong interest in theoretical studies concerning the phase coherence as well as the driving mechanism of the surface atom spins.[7,14−20] Despite its potential applications, this technique has barely been adopted so far.[21,22] In the case of single Fe atom ESR experiments, measurements were thus far only conducted in a magnetic field with a strong in-plane component at temperatures at or below 4 K[10,22] and with cabling that has high transmission in the radio frequency (RF) range.[21−23]

In this Letter, we explore the evolution of the resonance frequency and optimize the amplitude of the ESR signal by using an adjustable 2D vector magnetic field. We show that the strong in-plane magnetic field used previously is not essential. In addition, we show how to utilize the magnetic field from the spin-polarized STM tip (SP tip)[24−26] to assist the external field by adjusting the Zeeman-splitting and driving the ESR. Ultimately, we show that it is possible to perform single-atom ESR by using the tip field only. This eliminates the need of applying an external magnetic field. Furthermore, it relaxes the requirement for high-frequency cabling having good transmission over a wide range of frequencies, because it can operate at a single fixed radio frequency.

Received: August 29, 2019
Revised: October 22, 2019
Published: October 29, 2019

DOI: 10.1021/acs.nanolett.9b03559
Nano Lett. 2019, 19, 8201−8206

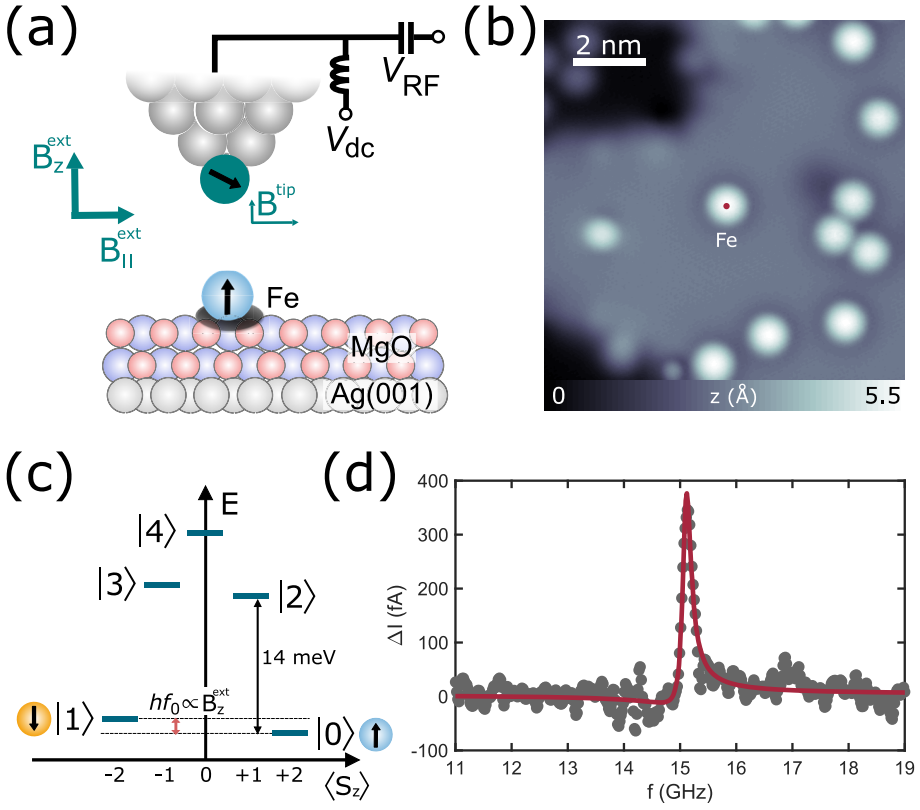

Figure 1. Electron spin resonance in a scanning tunneling microscope with a vector magnet. (a) Schematic of the experiment. Single Fe atoms on bilayer MgO grown on Ag(001) are studied using ESR-STM. An external vector magnet allows one to adjust the field in-plane $B_{\|}^{ext}$ and out-plane B_z^{ext} in addition to the field B^{tip} created by the spin-polarized magnetic tip. In addition to the dc bias voltage V_{dc}, a radio frequency (RF) voltage V_{RF} at frequency f is applied to the tunnel junction. (b) Constant-current topography showing several single atoms on an MgO surface, the central one being a Fe atom (I = 50 pA, V_{dc} = 60 mV, T = 0.9 K), (c) Energy level diagram of Fe on MgO showing the five lowest lying spin states.[7,27] B_z^{ext} splits the two lowest-lying spin states, $|0\rangle$ and $|1\rangle$, by hf_0, where h is Planck's constant. $B_{\|}^{ext}$ does not affect the Zeeman-splitting due to the large out-of-plane magnetic anisotropy of the spin system but increases the overlap in the spin components between $|0\rangle$ and $|1\rangle$.[7] The same holds for the components of the tip magnetic field. (d) ESR spectrum taken on the center of the Fe atom (red dot). Red line is a fitted Fano-Lorentzian curve. (I = 10 pA, V_{dc} = 40 mV, V_{RF} = 10 mV, T = 0.9 K, $B_{\|}^{ext}$ = 1.4 T, B_z^{ext} = 0.12 T).

Experiments were conducted in a commercial STM system (Unisoku USM1300) with a maximum external vector magnetic field of B_z^{ext} = 6 T and $B_{\|}^{ext}$ = 5 T (2 T in vector operation, STM temperature T = 0.3−1 K). The experimental setup is depicted in Figure 1a. The measurements were performed on well-isolated individual Fe atoms adsorbed atop two atomic layers of MgO grown on a Ag(100) substrate. Figure 1b shows a STM topography with a Fe atom in the center (energy level diagram in Figure 1c). We here follow the ESR implementation described in refs 7 and 23. (See Supporting Information for further details.) For ESR-STM measurements, an RF voltage V_{RF} is added to the direct current (dc) bias voltage V_{dc} and the radio frequency f is swept. This RF voltage drives transitions between the two lowest-lying Zeeman-split states of the Fe atom, and the change of state population is detected by a difference in tunneling current ΔI through tunneling magneto-resistance.[7] The Fe atoms on this surface have strong out-of-plane (z-axis, Figure 1c) anisotropy, so their resonance frequency is given by

$$f_0 = \frac{2\mu_{Fe}\cdot[B_z^{ext} + B_z^{tip}]}{h} \quad (1)$$

where μ_{Fe} is the magnetic moment of Fe, h is Planck's constant, and B_z^{ext} is the external magnetic field in the z-direction. B_z^{tip} is the z-axis component of the magnetic field generated by the SP tip,[24−26] which is made magnetic by picking up several Fe atoms (typically 1−3) from the surface.

Various theoretical proposals have addressed the mechanism of single-atom ESR.[7,14−20] Recent experiments, performed on Ti atoms on the surface, suggest that the atom is exposed to a time-varying tip magnetic field component perpendicular to the Zeeman field, similar to conventional ESR. This mechanism works because the atom is mechanically shaken on the polar surface of MgO by the oscillating V_{RF}. Consequently, the Rabi rate Ω, characterizing how fast a spin can be driven coherently, increases linearly with the tip magnetic field gradient.[26]

Figure 1d shows a typical ESR peak taken on a single Fe atom. The shape of the resonance is Lorentzian $\Delta I = I_{peak}\cdot[1 + \delta^2]^{-1}$, given by the steady-state solution of the Bloch equations[7] (see ref 11 for a detailed treatment of the Fano-shaped asymmetric contribution). Here, $\delta = 2(f - f_0)/\Gamma$ with Γ being the line width of the ESR peak. The ESR peak amplitude I_{peak} is determined by several experimental parameters[10]

$$I_{peak} = I\cdot 2\eta\cdot\left[P_0 - \frac{1}{2}\right]\cdot\Phi(\Omega) \quad (2)$$

Here, I is the dc tunneling current applied during an ESR sweep, η is the spin polarization of the tip, and P_0 is the

DOI: 10.1021/acs.nanolett.9b03559
Nano Lett. 2019, 19, 8201−8206

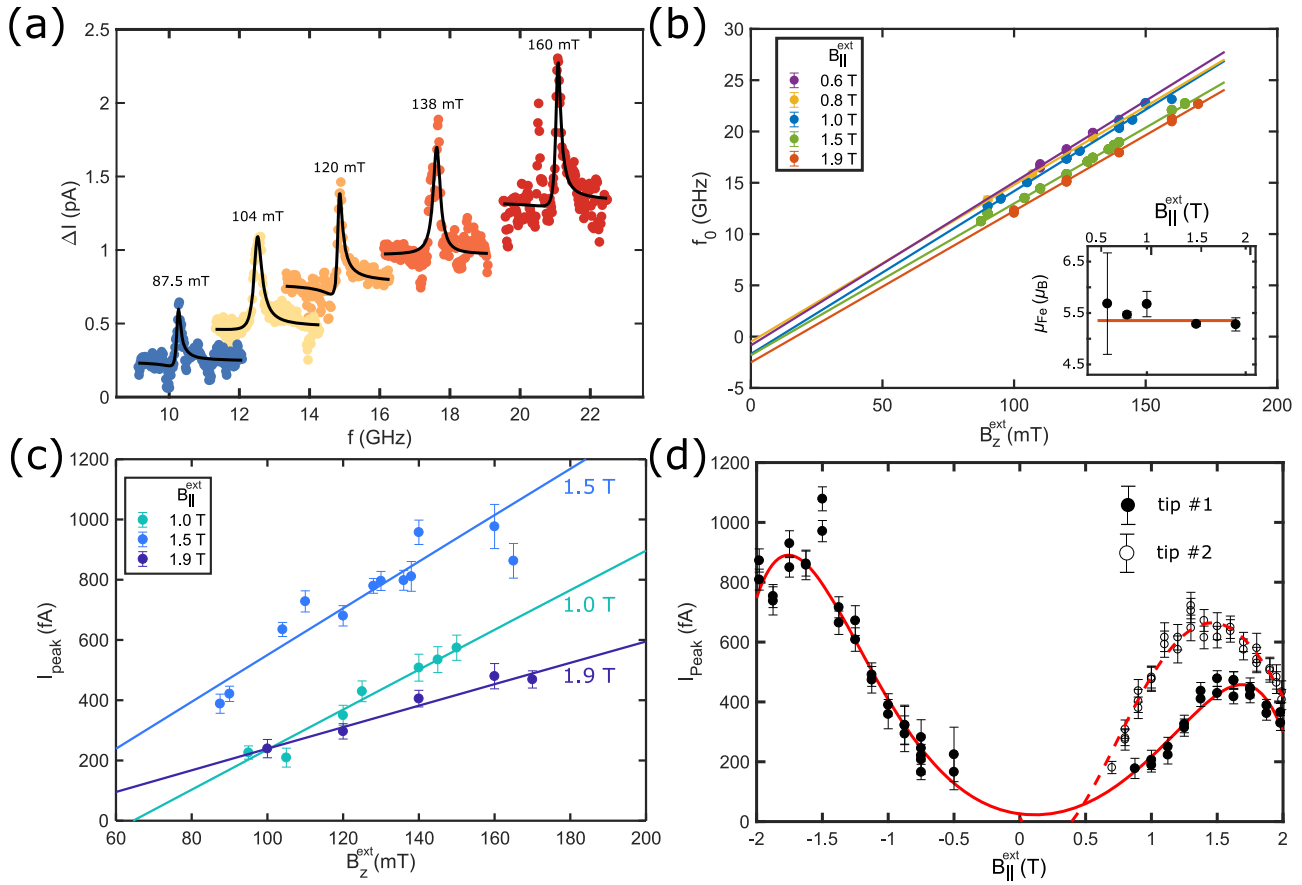

Figure 2. Magnetic-field dependence of single-atom ESR peaks. (a) ESR spectra taken on the Fe atom in Figure 1 for different external magnetic field B_z^{ext}. Plots are shifted vertically for clarity. (I = 50 pA, V_{dc} = 60 mV, V_{RF} = 22 mV, $B_{\parallel}^{ext}$ = 1.5 T, T = 0.8 K. Additional peak at 160 mT stems from a bad RF transmission at that frequency.) (b) Resonance frequencies f_0 as a function of B_z^{ext} for different $B_{\parallel}^{ext}$. Influence of the tip-magnetic field has been subtracted for all curves (see Supporting Information). Inset: Magnetic moment of Fe (μ_{Fe}), extracted from the slopes for each $B_{\parallel}^{ext}$ [eq 1]. Red line shows the mean value. (c) ESR peak amplitude I_{peak} as a function of B_z^{ext} for three $B_{\parallel}^{ext}$ and (d) as a function of $B_{\parallel}^{ext}$. In panel (d), all measurements were conducted at f_0 = 17 ± 0.5 GHz [red line: guide to the eye, I = 50 pA, V_{dc} = 60 mV, V_{RF} = 15 mV (tip #1), 22 mV (tip #2), T = 0.9 K]. Closed (open) circles are taken for tip #1 (tip #2).

ground-state population probability of the Fe spin when off-resonance. The driving factor $\Phi(\Omega) = T_1T_2\Omega^2/(1 + T_1T_2\Omega^2)$ ranges from 0 to 1 and characterizes how much the spin population is driven into equal state population. It depends on the Rabi rate Ω, the spin relaxation time T_1, and phase coherence time T_2 (see Supporting Information).

In the following, we make use of our 2D external magnetic field in order to analyze the change in the properties of the ESR signal. We measure ESR at tunneling conductances (σ = 50 pA/60 mV = 0.8 nS) that are comparable to those used in refs 7 and 10. For these tunneling conditions, we find that the z-axis component of the magnetic field from the SP tip (B_z^{tip}) is less than 10% of B_z^{ext}. Figure 2a shows ESR measurements as a function of B_z^{ext} at a fixed $B_{\parallel}^{ext}$ = 1.5 T. We find that f_0 shifts linearly with B_z^{ext}, as described by eq 1. This linear relation holds when the experiment is repeated for different $B_{\parallel}^{ext}$ as shown in Figure 2b. Given a strong out-of-plane magnetic anisotropy of Fe,[27] its magnetic moment does not align with the in-plane magnetic field. This explains the unchanged slope for varying $B_{\parallel}^{ext}$ and results in a constant magnetic moment of μ_{Fe} = (5.35 ± 0.14)μ_B (Figure 2, inset). This is in excellent agreement with previous works.[7,8,27] The lines deviate from the origin (B_z^{ext} = 0 and f_0 = 0) which is caused by a small misalignment [∼(1−2)°] between the sample and the magnetic field axes. This misalignment leads to an additional B_z^{ext} component when applying $B_{\parallel}^{ext}$. Measurements on different atoms revealed only small variations of ∼3% in f_0, in contrast to earlier reports[7] (see Supporting Information).

With the benefit of a 2D vector magnet, we now investigate the ESR peak amplitude I_{peak} as a function of B_z^{ext} and $B_{\parallel}^{ext}$. Figure 2a indicates that I_{peak} increases with B_z^{ext}. The peak amplitudes are plotted in Figure 2c for three different $B_{\parallel}^{ext}$. The increase with B_z^{ext} for a given $B_{\parallel}^{ext}$ is mainly caused by an improved ground-state population P_0 [eq 2], because the polarization into the ground state approximately follows $\left[P_0 - \frac{1}{2}\right] \propto B_z^{ext}$ (see Supporting Information). However, the peak amplitudes at different $B_{\parallel}^{ext}$ are strikingly different, which is shown in Figure 2d in greater detail. Overall, I_{peak} increases with in-plane magnetic field and is maximized at $B_{\parallel}^{ext} \approx \pm 1.5$ T.

For now, we cannot attribute the trend of the ESR peak amplitude to one dominant effect and it is likely that several factors are contributing. The monotonic increase of the ESR peak amplitude up to ∼1.5 T can be explained by an increased SP tip polarization η and an improved driving term $\Phi(\Omega)$ as evident from eq 2. Indeed, theoretical calculations suggest that a higher $B_{\parallel}^{ext}$ results in a higher Rabi rate Ω and therefore higher $\Phi(\Omega)$.[7,14] At $B_{\parallel}^{ext}$ exceeding ∼1.5 T, we find that the ESR peak amplitude decreases, which might be associated with

DOI: 10.1021/acs.nanolett.9b03559
Nano Lett. 2019, 19, 8201−8206

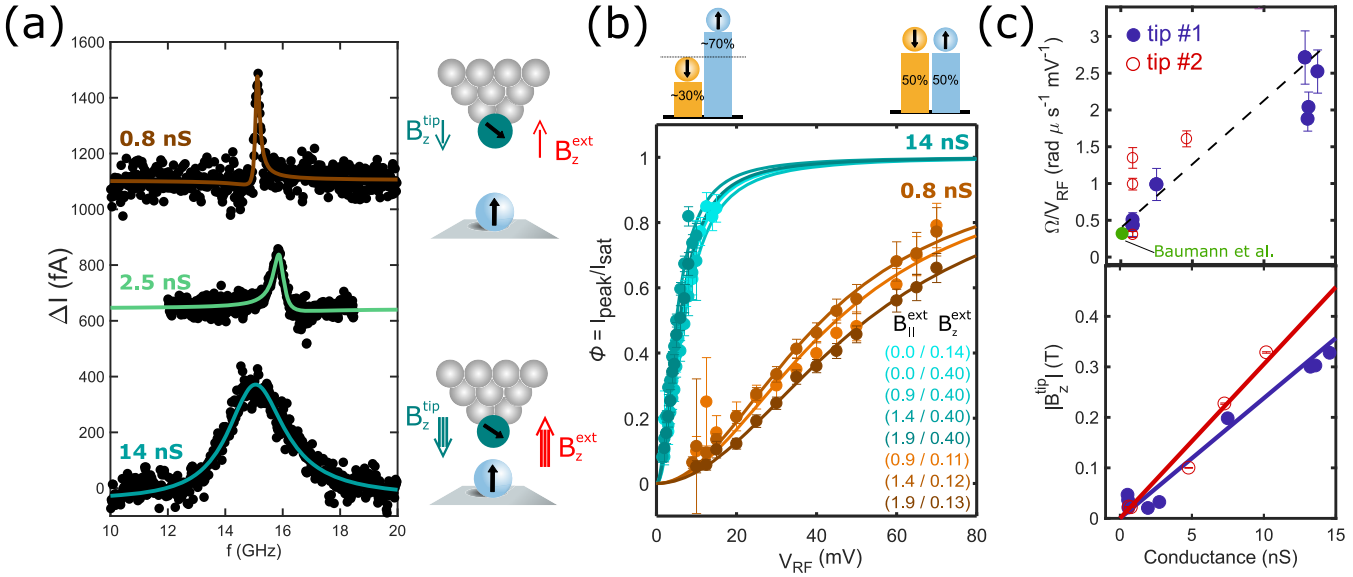

Figure 3. Improvement of the Rabi rate by increasing the tip field B^{tip}. (a) ESR spectra taken for different tunneling conductances and varying external magnetic field, illustrating that ESR at zero in-plane field is made possible by using higher conductance. (Tunneling parameters: top, I = 50 pA, V_{dc} = 60 mV, V_{RF} = 10 mV, $B_{\|}^{ext}$ = 1.4 T, B_z^{ext} = 0.12 T; middle, I = 20 pA, V_{dc} = −8 mV, V_{RF} = 8 mV, $B_{\|}^{ext}$ = 0 T, B_z^{ext} = 0.135 T; bottom: I = 115 pA, V_{dc} = 8 mV, V_{RF} = 3 mV, $B_{\|}^{ext}$ = 0 T, B_z^{ext} = 0.4 T. T = 1 K for all spectra. Curves have been offset vertically for clarity.) (b) Saturation measurements $\Phi(V_{RF}) = I_{peak}(V_{RF})/I_{sat}$ which give the ESR peak amplitude I_{peak} normalized to $I_{sat} = I{\cdot}2\eta{\cdot}\left[P_0 - \frac{1}{2}\right]$ (see eq 2 and ref 7). I_{sat} is the maximum value of I_{peak} in the limit of large V_{RF}, obtained when the spin system is saturated (driven to a 50%/50% state population $[\Phi(\Omega) = 1]$ as indicated in the sketch above). Colors indicate different external magnetic field settings as specified in the inset (Units in [T]). (c) Top: Rabi rate Ω normalized by the RF voltage (V_{RF}) for different tunneling conductances $\sigma = I/V_{dc}$. Green dot marks the value obtained in refs 7 and 10. Closed (open) circles are for tip #1 (#2). Dashed line is a guide to the eye. Bottom: z-component of the tip field $B_z^{tip}(\sigma)$ (see Supporting Information). The solid lines are linear fits to the data.

a decrease of spin relaxation time T_1, a trend that we find in pump−probe spectroscopy measurements (Supporting Information).

We have not observed any ESR signal for $B_{\|}^{ext} < 0.5$ T at small tunneling conductance σ in the range of 0.8 nS. This may be associated either with the tip's spin polarization being too low, or a strongly diminished Rabi rate. Interestingly, we successfully recover the ESR signal by increasing the tunneling conductance σ in the STM junction as shown in Figure 3a. As the STM tip gets closer to the Fe atom, we find that its stray magnetic field B_z^{tip} shifts the resonance of the Fe atom to lower frequencies. Subsequently, we compensate the shift of f_0 by increasing B_z^{ext} and thus maintain the resonance frequency constant (∼15 GHz). In the case of higher conductance (stronger tip field), we obtain an ESR signal even when lowering $B_{\|}^{ext}$ down to 0 T (Figure 3a). This suggests that the increased tip magnetic field facilitates driving ESR under these conditions.

As the conductance increases, the line width of the resonance becomes broader as well. This is likely caused by a decrease in T_2,[10] as well as mechanical vibrations of the tip, which lead to fluctuations in B_z^{tip}.[7] Nevertheless, we find that for higher conductances ESR can be readily obtained even though the RF voltage is low. This is manifested in Figure 3b, showing the driving factor $\Phi(\Omega)$ defined in eq 2 as a function of V_{RF} for various conductances and B^{ext} field configurations. Accordingly, we find that the ESR signal saturates at much lower RF voltages V_{RF} as the conductance is increased (Figure 3b, see Supporting Information and ref 10). The saturation curves show negligible dependence on $B_{\|}^{ext}$, indicating that the tip field dominates the saturation. To obtain the Rabi rate Ω from these measurements, T_1 and T_2 need to be determined under the respective tunneling parameters. Here, we estimate them using T_1 measurements under different parameters in combination with relations for T_1 and T_2 found previously[10,28] (Supporting Information).

The extracted Ω as a function of σ is shown in Figure 3c. Because Ω scales linearly with V_{RF},[7,10,14] we normalize the Rabi rate Ω/V_{RF} to obtain a measure of the driving efficiency. In addition, we plot the change in tip field B_z^{tip} projected onto the z-axis as a function of σ (evaluation see Supporting Information).

The two proportionalities $\Omega \propto \sigma$ and $B_z^{tip} \propto \sigma$ found here imply $\Omega \propto B_z^{tip}$. However, other measurements and theoretical models suggest an improvement in Ω for an increasing magnetic field gradient $\partial B_z^{tip}/\partial z$.[14,26] Still, this can be easily fulfilled in the case of magnetic exchange coupling, because of the exponential distance dependence that is proportional to its own derivative (Supporting Information).

These results indicate that a magnetic tip field can drive single-atom ESR. However, we cannot fully exclude the possibility of a crystal field driving mechanism as originally proposed in ref 7, because the electric field in the tunnel junction also increases for higher conductance.

Nevertheless, we achieve Rabi rates Ω on Fe atoms approximately 1 order of magnitude higher than previous experiments[7,10] (Figure 3c) by utilizing the proximity of the tip. We note that in the case of spin-1/2 Ti atoms, comparable Ω have been obtained.[26] In that case, the absence of an anisotropy barrier facilitates driving of Ti atoms but at the same time limits their T_1 to ∼100 ns.[9] In contrast, Fe atoms revealed a T_1 that is 3 orders of magnitude higher.[7,28]

Lastly, we demonstrate ESR on individual Fe atoms without any external magnetic field $B_{\|}^{ext} = B_z^{ext} = 0$ T by employing the

DOI: 10.1021/acs.nanolett.9b03559
Nano Lett. 2019, 19, 8201−8206

tip field to give the Zeeman splitting (Figure 4a). The resonance frequency shifts up for increasing conductance σ,

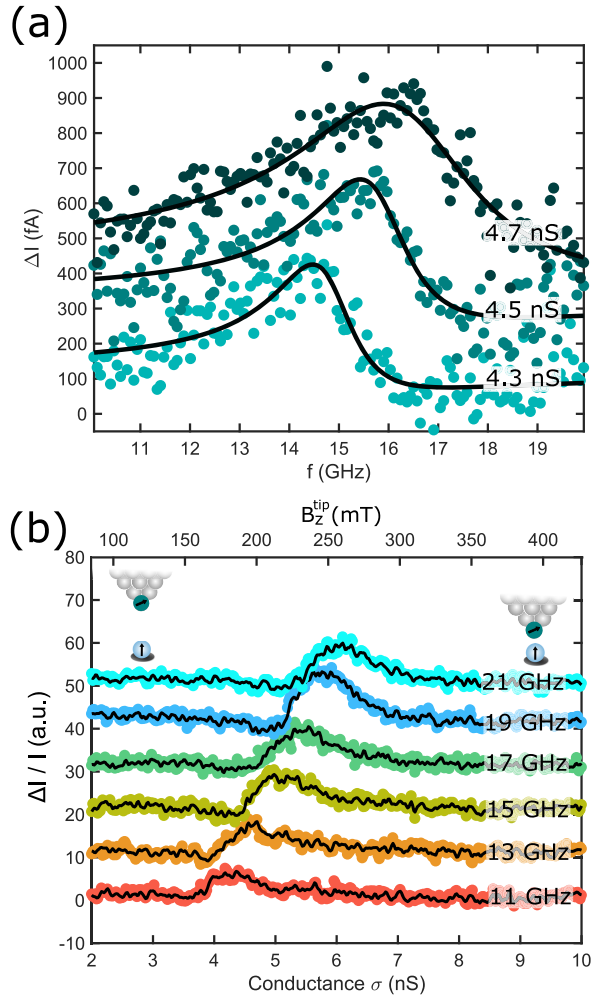

Figure 4. ESR without external magnetic field. (a) ESR spectra taken at zero external magnetic field $B_{\parallel}^{ext} = B_z^{ext} = 0$ T for different conductances σ (V_{dc} = 30 mV, V_{RF} = 15 mV, T = 0.4 K). Spectra shift in frequency due to the increasing magnetic field from the tip. Vertical offsets are added for clarity. (b) ESR spectrum for different fixed frequencies measured by sweeping the conductance σ (I = 100−500 pA, V_{dc} = 50 mV, V_{RF} = 25 mV). This effectively increases the tip field $B_z^{tip} \propto \sigma$ (top scale). ESR signal ΔI is normalized to compensate for the linear increase with I [See eq 2]. Vertical offsets have been added for clarity and a nonlinear background was subtracted (see Supporting Information).

because $B_z^{tip} \propto \sigma$. The ESR peak is even broader than those in Figure 3a, likely due to current-induced relaxation and decoherence.[10,28] As a consequence, our frequency range is now too narrow to reveal the full ESR peak. Therefore, we ultimately switch from sweeping f to sweeping the conductance σ at a fixed frequency whereas the current feedback loop remains enabled. Thus, the tip approaches the atom establishing a sweep in B_z^{tip}. This is demonstrated in Figure 4b where we perform tip-field ESR sweeps. As expected, the resonance linearly shifts to higher tunneling conductances for increasing set point frequency [eq 1]. In contrast to the broad ESR signal as a function of frequency (Figure 4a), this method offers a significantly larger range of ∼300 mT tip magnetic field which would capture a frequency window of equivalently ∼40 GHz. It also allows for a considerable speed-up of the measurement, because the tip magnetic field can be changed much faster (>1 kHz) than the frequency of the RF generator (<10 Hz). Moreover, this technique paves the way to perform ESR in STM systems without a magnetic field. In that case, a known reference system would be required to gauge the tip magnetic field, such as the Fe atom in this study or other magnetic atoms.[9,13] Alternatively, we here calibrate the tip field by only applying a small magnetic field of 50 mT and observing the change in the ESR position (see Supporting Information).

Our work illustrates how to tune the ESR properties by combining vector magnet and tip field and eventually realize single-atom ESR with tip field only. This suggests a way to study nanoscale magnetic systems revealing, for instance, magnetic bistability[29,30] and quantum tunneling of magnetization[31] in the absence of an external field. Moreover, demonstrating ESR-STM in a commercially available STM will allow this technique to be performed in a greater class of STM systems, even those without an external magnetic field.

■ ASSOCIATED CONTENT

Supporting Information

The Supporting Information is available free of charge on the ACS Publications website at DOI: 10.1021/acs.nanolett.9b03559.

sample preparation and experimental methods, ESR measurements on different atoms, pump−probe spectroscopy measurements, discussion on the peak height intensity, estimation of the Rabi rate, evaluation of the tip magnetic field as a function of conductance, discussion on the relation between Rabi rate and tip field, and the evaluation and supplemental data on the ESR without macroscopic field (PDF)

■ AUTHOR INFORMATION

Corresponding Authors

*E-mail: choi.taeyoung@qns.science.

*E-mail: heinrich.andreas@qns.science.

ORCID

Aparajita Singha: 0000-0001-6301-0394

Author Contributions

⊥P.W. A.S., and X.Z. contributed equally to this work.

Author Contributions

P.W., A.S., X.Z., T.E., and T.C. performed the experiments. T.C. and A.J.H. supervised the project. P.W. wrote the manuscript with contributions from all authors. All authors discussed the results.

Notes

The authors declare no competing financial interest.

■ ACKNOWLEDGMENTS

All authors acknowledge support from the Institute for Basic Science under Grant IBS-R027-D1. P.W. acknowledges support from the Alexander von Humboldt Foundation. We acknowledge Minhee Choi for fruitful discussions. We also thank William Paul for providing software to control the RF source.

■ REFERENCES

(1) Balasubramanian, G.; Chan, I. Y.; Kolesov, R.; Al-Hmoud, M.; Tisler, J.; Shin, C.; Kim, C.; Wojcik, A.; Hemmer, P. R.; Krueger, A.;

DOI: 10.1021/acs.nanolett.9b03559
Nano Lett. 2019, 19, 8201−8206

Hanke, T.; Leitenstorfer, A.; Bratschitsch, R.; Jelezko, F.; Wrachtrup, J. Nanoscale imaging magnetometry with diamond spins under ambient conditions. *Nature* **2008**, *455*, 648−651.
(2) Rugar, D.; Budakian, R.; Mamin, H. J.; Chui, B. W. Single spin detection by magnetic resonance force microscopy. *Nature* **2004**, *430*, 329−332.
(3) Degen, C. L.; Poggio, M.; Mamin, H. J.; Rettner, C. T.; Rugar, D. Nanoscale magnetic resonance imaging. *Proc. Natl. Acad. Sci. U. S. A.* **2009**, *106*, 1313−1317.
(4) Gross, I.; Akhtar, W.; Garcia, V.; Martínez, L. J.; Chouaieb, S.; Garcia, K.; Carrétéro, C.; Barthélémy, A.; Appel, P.; Maletinsky, P.; Kim, J. V.; Chauleau, J. Y.; Jaouen, N.; Viret, M.; Bibes, M.; Fusil, S.; Jacques, V. Real-space imaging of non-collinear antiferromagnetic order with a single-spin magnetometer. *Nature* **2017**, *549*, 252−256.
(5) Casola, F.; van der Sar, T.; Yacoby, A. Probing condensed matter physics with magnetometry based on nitrogen-vacancy centres in diamond. *Nat. Rev. Mater.* **2018**, *3*, 17088.
(6) Thiel, L.; Wang, Z.; Tschudin, M. A.; Rohner, D.; Gutiérrez-Lezama, I.; Ubrig, N.; Gibertini, M.; Giannini, E.; Morpurgo, A. F.; Maletinsky, P. Probing magnetism in 2D materials at the nanoscale with single spin microscopy. *Science* **2019**, *364*, 973−976.
(7) Baumann, S.; Paul, W.; Choi, T.; Lutz, C. P.; Ardavan, A.; Heinrich, A. J. Electron paramagnetic resonance of individual atoms on a surface. *Science* **2015**, *350*, 417−420.
(8) Choi, T.; Paul, W.; Rolf-Pissarczyk, S.; Macdonald, A. J.; Natterer, F. D.; Yang, K.; Willke, P.; Lutz, C. P.; Heinrich, A. J. Atomic-scale sensing of the magnetic dipolar field from single atoms. *Nat. Nanotechnol.* **2017**, *12* (5), 420−424.
(9) Yang, K.; Bae, Y.; Paul, W.; Natterer, F. D.; Willke, P.; Lado, J. L.; Ferrón, A.; Choi, T.; Fernández-Rossier, J.; Heinrich, A. J.; Lutz, C. P. Engineering the eigenstates of coupled spin-1/2 atoms on a surface. *Phys. Rev. Lett.* **2017**, *119*, 227206.
(10) Willke, P.; Paul, W.; Natterer, F. D.; Yang, K.; Bae, Y.; Choi, T.; Fernández-Rossier, J.; Heinrich, A. J.; Lutz, C. P. Probing quantum coherence in single-atom electron spin resonance. *Science Adv.* **2018**, *4* (2), eaaq1543.
(11) Bae, Y.; Yang, K.; Willke, P.; Choi, T.; Heinrich, A. J.; Lutz, C. P. Enhanced quantum coherence in exchange coupled spins via singlet-triplet transitions. *Science Adv.* **2018**, *4* (11), eaau4159.
(12) Willke, P.; Bae, Y.; Yang, K.; Lado, J. L.; Ferrón, A.; Choi, T.; Ardavan, A.; Fernández-Rossier, J.; Heinrich, A. J.; Lutz, C. P. Hyperfine interaction of individual atoms on a surface. *Science* **2018**, *362* (6412), 336−339.
(13) Yang, K.; Willke, P.; Bae, Y.; Ferrón, A.; Lado, J. L.; Ardavan, A.; Fernández-Rossier, J.; Heinrich, A. J.; Lutz, C. P. Electrically controlled nuclear polarization of individual atoms. *Nat. Nanotechnol.* **2018**, *13* (12), 1120−1125.
(14) Lado, J. L.; Ferrón, A.; Fernández-Rossier, J. Exchange mechanism for electron paramagnetic resonance of individual adatoms. *Phys. Rev. B: Condens. Matter Mater. Phys.* **2017**, *96* (20), 205420.
(15) Shakirov, A. M.; Rubtsov, A. N.; Ribeiro, P. Spin transfer torque induced paramagnetic resonance. *Phys. Rev. B: Condens. Matter Mater. Phys.* **2019**, *99* (5), No. 054434.
(16) Berggren, P.; Fransson, J. Electron paramagnetic resonance of single magnetic moment on a surface. *Sci. Rep.* **2016**, *6*, 25584.
(17) Shavit, G.; Horovitz, B.; Goldstein, M. Generalized open quantum system approach for the electron paramagnetic resonance of magnetic atoms. *Phys. Rev. B: Condens. Matter Mater. Phys.* **2019**, *99* (19), 195433.
(18) Delgado, F.; Fernández-Rossier, J. Spin decoherence of magnetic atoms on surfaces. *Prog. Surf. Sci.* **2017**, *92* (1), 40−82.
(19) Ibañez-Azpiroz, J.; dos Santos Dias, M.; Blügel, S.; Lounis, S. Longitudinal and transverse spin relaxation times of magnetic single adatoms: An ab initio analysis. *Phys. Rev. B: Condens. Matter Mater. Phys.* **2017**, *96* (14), 144410.
(20) Gálvez, J. R.; Wolf, C.; Delgado, F.; Lorente, N. Cotunneling mechanism for all-electrical electron spin resonance of single adsorbed atoms. *Phys. Rev. B: Condens. Matter Mater. Phys.* **2019**, *100* (3), No. 035411.
(21) Natterer, F. D.; Patthey, F.; Bilgeri, T.; Forrester, P. R.; Weiss, N.; Brune, H. Upgrade of a low-temperature scanning tunneling microscope for electron-spin resonance. *Rev. Sci. Instrum.* **2019**, *90* (1), No. 013706.
(22) Seifert, T. S.; Kovarik, S.; Nistor, C.; Persichetti, L.; Stepanow, S.; Gambardella, P. Single-atom electron paramagnetic resonance in a scanning tunneling microscope driven by a radiofrequency antenna at 4 K. arXiv preprint 2019, arXiv:1908.03379.
(23) Paul, W.; Baumann, S.; Lutz, C. P.; Heinrich, A. J. Generation of constant-amplitude radio-frequency sweeps at a tunnel junction for spin resonance STM. *Rev. Sci. Instrum.* **2016**, *87*, No. 074703.
(24) Yan, S.; Choi, D. J.; Burgess, J. A.; Rolf-Pissarczyk, S.; Loth, S. Control of quantum magnets by atomic exchange bias. *Nat. Nanotechnol.* **2015**, *10* (1), 40−45.
(25) Willke, P.; Yang, K.; Bae, Y.; Heinrich, A. J.; Lutz, C. P. Magnetic Resonance Imaging of Single Atoms. *Nat. Phys.* **2019**, *15*, 1005.
(26) Yang, K.; Paul, W.; Natterer, F. D.; Lado, J. L.; Bae, Y.; Willke, P.; Choi, T.; Ferrón, A.; Fernández-Rossier, J.; Heinrich, A. J.; Lutz, C. P. Tuning the Exchange Bias on a Single Atom from 1 mT to 10 T. *Phys. Rev. Lett.* **2019**, *122* (22), 227203.
(27) Baumann, S.; Donati, F.; Stepanow, S.; Rusponi, S.; Paul, W.; Gangopadhyay, S.; Rau, I. G.; Pacchioni, G. E.; Gragnaniello, L.; Pivetta, M.; Dreiser, J.; Piamonteze, C.; Lutz, C. P.; Macfarlane, R. M.; Jones, B. A.; Gambardella, P.; Heinrich, A. J.; Brune, H. Origin of perpendicular magnetic anisotropy and large orbital moment in Fe atoms on MgO. *Phys. Rev. Lett.* **2015**, *115* (23), 237202.
(28) Paul, W.; Yang, K.; Baumann, S.; Romming, N.; Choi, T.; Lutz, C. P.; Heinrich, A. J. Control of the millisecond spin lifetime of an electrically probed atom. *Nat. Phys.* **2017**, *13*, 403−407.
(29) Khajetoorians, A. A.; Baxevanis, B.; Hübner, C.; Schlenk, T.; Krause, S.; Wehling, T. O.; Lounis, S.; Lichtenstein, A.; Pfannkuche, D.; Wiebe, J.; Wiesendanger, R. Current-driven spin dynamics of artificially constructed quantum magnets. *Science* **2013**, *339* (6115), 55−59.
(30) Loth, S.; Baumann, S.; Lutz, C. P.; Eigler, D. M.; Heinrich, A. J. Bistability in atomic-scale antiferromagnets. *Science* **2012**, *335* (6065), 196−199.
(31) Forrester, P. R.; Patthey, F.; Fernandes, E.; Sblendorio, D. P.; Brune, H.; Natterer, F. D. A quantum pathway to overcome the trilemma of magnetic data storage. arXiv preprint 2019, arXiv:1903.00242.

DOI: 10.1021/acs.nanolett.9b03559
Nano Lett. 2019, 19, 8201−8206